INTERNATIONAL JOURNAL OF
NUMERICAL ANALYSIS AND MODELING
Volume 22, Number 1, Pages 96–112

doi: 10.4208/ijnam2025-1005

A DIFFERENCE VIRTUAL ELEMENT METHOD FOR THE 3D ELLIPTIC EQUATION WITH THE VARIABLE COEFFICIENT ON GENERAL CYLINDRICAL DOMAINS

LULU LI, YINNIAN HE, AND XINLONG FENG

Abstract. In this paper, we present and analysis a difference virtual element method (DVEM) for the three dimensional (3D) elliptic equation on general cylindrical domains. This method combines the dimension splitting method and operator splitting technique to transform the virtual element solution of 3D elliptic equation into a series of virtual element solution of 2D elliptic equation based on (x, y) plane, where the central difference discretization is adopted in the z-direction. This allows us to solve partial differential equations on cylindrical domains at the low cost in mesh generation compared with 3D virtual element method. The H^1-norm error estimation of the DVEM is analysed in this paper. Finally, some numerical examples are performed to verify the theoretical predictions and showcase the efficiency of the proposed method.

Key words. 3D elliptic equation, difference virtual element, virtual element, cylindrical domain, error analysis.

1. Introduction

The development of the numerical methods for the 3D partial differential equation on general polygonal (polyhedral) meshes has been drawn considerable attention due to the extensive flexibility for the polygonal (polyhedral) meshes on the mesh generation, mesh deformation, fracture, combination, topology optimization, and mesh refinement and coarsening. In addition, the use of arbitrary-shape meshes can have good flexibility in dealing with complex data features. With regards to the spatial discretization, there exist many works devoted to treating the general polygonal and polyhedral elements. These methods include the finite volume method [1, 2], weak Galerkin finte element method, mimetic finite difference method [3] and the virtual element method (VEM) [4, 5, 6, 7].

The virtual element method was originally proposed in [8] to solve the Poisson equation and later has been successfully applied to a variety of partial differential equations such as convection diffusion equation, Allen-Cahn equation, Cahn Hilliard equation. More recently, mixed VEM was proposed for solving the fluid flow problems, see the Stokes problem [9, 10], Brinkman problem [11, 12], Stokes-Darcy problem [13, 14], Stokes complex in the VEM framework [15, 16], the magnetohydrodynamics problems [17] and the steady quasi-geostrophic equation of the ocean [18]. Several studies have contributed to the development and refinement of VEM for elliptic interface problems. For instance, Cao et al. [19] introduced immersed virtual element methods for two-dimensional elliptic interface problems. Chen et al. [20] focused on an interface-fitted mesh generator and virtual element methods for elliptic interface problems. Gómez et al. [21] explored space-time virtual elements for the heat equation. Their work extended the concept of VEM to evolve problems in time, which is particularly useful for capturing the temporal behavior of interfaces. Tushar et al. [22] investigated virtual element methods for general linear elliptic interface problems on polygonal meshes with small edges. Wang et

Received by the editors on February 22, 2024 and, accepted on September 5, 2024.
2000 *Mathematics Subject Classification.* 65N06, 65N15, 65N50.

al. [23] introduced a conforming virtual element method based on unfitted meshes for the elliptic interface problem.

The finite difference method, as an important numerical method, plays a crucial role in scientific calculating [24, 25, 26, 27]. However, the finite difference method is not easy to discretize the complex domain,especially in high dimensional space. Dimension splitting method [28, 29, 30, 31, 32, 30] and operator splitting method are two popular strategies to reduce the high dimensional problem into a series of low-dimensional problems. Based on the idea of dimension splitting method and operator splitting technique, He and Feng proposed the difference finite element method (DFEM) for solving 3D partial differential equations. In [33], the author used the DFEM based on P_1-P_1 conforming elements to solve the 3D Poisson equation and obtained the H^1 superconvergence results of this method by quadratic interpolation. In addition, Feng and his collaborators applied the DFEM to solve the 3D heat conduction equation [34] and obtained the H^1-superconvergence results. Later in [35, 36, 37] , they proceeded the DFEM to solve the 3D continuous incompressible Stokes equations and Navier-Stokes equations and obtained the existence, uniqueness and stability of the finite element solution as well as the optimal convergence.

For $L_3 > 0$, let $\Omega = \omega \times (0, L_3)$ where $\omega \subset \mathbb{R}^2$. We consider the following 3D elliptic equation with Dirichlet boundary condition:

$$\begin{cases} -\widetilde{\nabla} \cdot (\widetilde{\mathbf{A}} \widetilde{\nabla} u) := -\partial_{zz} u - \nabla \cdot (\mathbf{A}(x,y) \nabla u) = f & \text{in } \Omega, \\ u = 0 & \text{on } \partial\Omega, \end{cases} \tag{1}$$

where $\widetilde{\nabla} = (\partial_x, \partial_y, \partial_z) = (\nabla, \partial_z)$ and $\tilde{\mathbf{A}} \in [L^\infty(\Omega)]^{3\times 3}$ is the symmetric matrix-value function of form

$$\widetilde{\mathbf{A}} = \begin{pmatrix} \mathbf{A}(x,y) & 0 \\ 0 & 1 \end{pmatrix}.$$

Here $\mathbf{A}(x,y) \in [L^\infty(\omega)]^{2\times 2} = \begin{pmatrix} A_{11}(x,y) & A_{12}(x,y) \\ A_{21}(x,y) & A_{22}(x,y) \end{pmatrix}$ is assumed to be uniformly elliptic and continuous in the sense that there exist two positive constants $0 < \alpha_* \leq \alpha^* < +\infty$ such that

$$\alpha_* |\boldsymbol{\xi}|^2 \leq \sum_{i,j=1}^{2} A_{ij}(x,y) \xi_i \xi_j \leq \alpha^* |\boldsymbol{\xi}|^2 \quad \forall (x,y) \in \omega,$$

for any $\boldsymbol{\xi} = (\xi_1, \xi_2)^\top \in \mathbb{R}^2$.

This manuscript introduces a novel DVE approach grounded in lower-order elements for resolving 3D elliptic equations. By preserving the virtues of the virtual element method, the computational demands of intricate 3D scenarios are substantially reduced. The underlying principle of this DVE strategy involves utilizing finite difference method discretization in the z-direction to convert the 3D model into a collection of 2D elliptic equations, which are then approximated using the low-order virtual element method in the (x, y) plane. Consequently, the numerical solution to a complex 3D problem can be obtained by combining the numerical solutions of several 2D problems. Although the dimension of the coefficient matrix presented by the difference virtual element method remains unchanged, the stiffness matrix can be reused at each z-grid point without the need for reassembly, thereby conserving computational resources.

The structure of this article is as follows. In the next section, we introduce the virtual element space and the method of virtual elements in the 2D domain. In

Section 3, we introduce the DVE methods for the 3D elliptic equation. Then the stability and error results of the DVE methods are given. Finally, numerical results validate the error order and effectiveness of the DVE.

2. Virtual element method for 2D elliptic equation

In this section, we consider the following 2D elliptic equation with Dirichlet boundary condition defined in convex polygon domain $\omega \subset \mathbb{R}^2$,

$$\begin{cases} -\nabla \cdot (\mathbf{A}(x,y)\nabla u) = f & \text{in } \omega, \\ u = 0 & \text{on } \partial\omega. \end{cases} \tag{2}$$

The variational form of ((2)) is to find $u \in H_0^1(\omega) := \{w \in H^1(\omega) : w = 0 \text{ on } \partial\omega\}$ by solving

$$a(u,v) = (f,v)_{0,\omega} \quad \forall v \in H_0^1(\omega), \tag{3}$$

where $a(u,v)$ is the bilinear form defined by

$$a(u,v) = (\mathbf{A}(x,y)\nabla u, \nabla v)_{0,\omega} \tag{4}$$

and $(\cdot,\cdot)_{0,\omega}$ denotes the L^2 inner product on ω with the induced norm $\|\cdot\|_{0,\omega}$. Alternatively, we denote by $\|\cdot\|_{m,\omega}$ the norm defined in the Hilbert space $H^m(\omega)(m \in \mathbb{Z}^+)$ with the corresponding seminorm $|\cdot|_{m,\omega}$.

2.1. Virtual element space. Considering a partition $\mathcal{T}_h$ of ω into non-overlapping polygonal meshes with a maximum diameter of h, we assume the presence of a positive constant ρ, independent of E, that fulfills the following criteria: (i) every element E is star-shaped with respect to every point inside a disk with a radius of at least ρh_E; (ii) the length of every edge e within E is greater than or equal to ρh_E. For each element E in $\mathcal{T}_h$, $\mathbf{x}_E$ represents the centroid, h_E denotes the diameter, and $|E|$ indicates the measure of E. Let $\mathbb{P}_s(E)$ be the space of polynomials of degree less than or equal to s in E with the dimension

$$n_s := \dim\mathbb{P}_s(E) = \frac{(s+1)(s+2)}{2}.$$

In this paper, we restrict our focus on the case $s = 1$, i.e., the lower-order polynomials. In classical finite element methods, it is not easy to find explicit expressions for low order basis functions on more general polyhedral elements. The virtual element method circumvents this difficulty, and ultimately lists computable stiffness matrices. Inspired by [8], we define a local finite dimensional space $W_h(E)$ on each polygon E:

$$W_h(E) = \left\{v_h \in H^1(E) : v_h|_{\partial E} \in C^0(\partial E) : v_h|_e \in \mathbb{P}_1(e), \forall e \in \partial E, \Delta v_h \in \mathbb{P}_1(E)\right\}.$$

It is easy to see that $\mathbb{P}_1(E) \subset W_h(E)$. Then we provide a computable basis function, namely the scaled:

$$\mathcal{M}_1(E) := \{1, \frac{x - x_E}{h_E}, \frac{y - y_E}{h_E}\},$$

where $\mathbf{x}_E = (x_E, y_E)$ is the centroid of E. Obviously, $\mathcal{M}_1(E)$ is a set of basis functions for $\mathbb{P}_1(E)$.

Due to the low order virtual element method used in this article, only the element nodes are required for the degrees of freedom. According to [8], we introduce the degree of freedom in $V_h^E(E)$: The value of v_h at the vertices of E.

Next, we define the projection operator $\Pi_E^\nabla : W_h(E) \to \mathbb{P}_1(E)$:

$$\begin{cases} (\mathbf{A}(x,y)\nabla(\Pi_E^\nabla v_h - v_h), \nabla p)_{0,E} = 0 \quad \forall p \in \mathbb{P}_1(E), \\ \overline{\Pi_E^\nabla v_h} = \overline{v_h}, \end{cases} \tag{5}$$

where $\overline{v_h} := \frac{1}{n_E}\sum_{i=1}^{n_E} v_h(\mathbf{x}_i)$ denotes the average value of w_h at the vertices of the polygon element E with n_E being the number of the vertices of polygon element E. The second equation is used to fix the constant part of $\Pi_E^\nabla v_h$. Noting that $\Pi_E^\nabla v_h$ can be indeed calculated from its degrees of freedom. Obviously, according to the divergence theorem, there holds that for any $v_h \in W_h$ and $p \in \mathbb{P}_1(E)$,

$$(\mathbf{A}(x,y)\nabla\Pi_E^\nabla v_h, \nabla p)_{0,E} = (\mathbf{A}(x,y)\nabla v_h, \nabla p)_{0,E} = \sum_{e\in\partial E}\int_e \mathbf{A}(x,y)v_h\mathbf{n}_e \cdot \nabla p ds, \tag{6}$$

where we have used that the Laplacian value of a linear function vanishes. $\mathbf{n}_e$ is the unit normal vector to the edge e pointing out of the element E. It follows from the definition of the local virtual element space W_h that we can calculate the right-hand end of equation (6) exactly, since the gradient of the linear polynomial p is a known constant.

Next the local and global conforming virtual element spaces can be defined as follows:

$$V_h^E(E) := \left\{ v_h \in W_h(E) : \int_E v_h p dx = \int_E \Pi_E^\nabla v_h p dx, \ \forall p \in \mathbb{P}_1(E) \right\},$$
$$V_h(\Omega) := \left\{ v_h \in H_0^1(\Omega) : v_h|_E \in V_h^E(E), \ \forall E \in \mathcal{T}_h \right\}.$$

2.2. Discrete scheme. Define the bilinear form $a^E : H^1(E) \times H^1(E) \to \mathbb{R}$

$$a(u,v) := \sum_{E\in\mathcal{T}_h} a^E(u,v),$$

following [8], we introduce the discrete counterpart $a_h^E : V_h^E \times V_h^E \to \mathbb{R}$ of a^E:

$$a_h^E(v_h, w_h) := (\mathbf{A}(x,y)\nabla\Pi_E^\nabla v_h, \nabla\Pi_E^\nabla w_h) + S^E(v_h - \Pi_E^\nabla v_h, w_h - \Pi_E^\nabla w_h),$$

where S^E is a symmetric bilinear form called the stabilization term and satisfies that there exist two uniform constants α_* and α^* such that

$$\alpha_*|v_h|^2 \le S^E(v_h, v_h) \le \alpha^*|v_h|^2, \quad \forall v_h \in V_h(E) \quad \text{with} \quad \Pi_E^\nabla v_h = 0.$$

Thus S^E can be approximated by

$$S^E(v_h, w_h) := \sum_{r=1}^{n_E} \mathrm{dof}_r(v_h)\mathrm{dof}_r(w_h), \tag{7}$$

where $\mathrm{dof}_r(v_h)$ denotes the value of $v_h \in V_h^E$ in the r-th local degree of freedom. Therefore, (7) can be calculated directly from the degrees of freedom. To this end, $a_h^E(\cdot,\cdot)$ preserves the stability, there exist two positive constants α_1, α_2 independent of h and E such that

$$\alpha_1 a^E(v_h, v_h) \le a_h^E(v_h, v_h) \le \alpha_2 a^E(v_h, v_h) \quad \forall v_h \in V_h^E(E).$$

Finally, we define

$$a_h(v_h, w_h) := \sum_{E\in\mathcal{T}_h} a_h^E(v_h, w_h),$$

to be the global approximate form of $a(\cdot,\cdot)$.

Denote by $\Pi_E^1 : V_h^E(E) \to \mathbb{P}_1(E)$ the L^2-orthogonal projection onto $\mathbb{P}_1(E)$

$$(v_h, p)_{0,E} = (\Pi_E^1 v_h, p)_{0,E}, \forall p \in \mathbb{P}_1(E).$$

Note that when $s = 1$, $\Pi_E^1 = \Pi_E^\nabla$ for the enhanced virtual element space

$$\widetilde{V}_h^E = \left\{ w \in H^1(E) : w|_{\partial E} \in \mathbb{P}_1(\partial E),\ \Delta w \in \mathbb{P}_1(E) \right\},$$

which has the same degrees of freedom as in V_h^E, thus $\Pi_E^1 v_h$ is also computable. Then we define the discrete counterpart of local L^2 inner produce in E

$$(v_h, w_h)_{h,E} := (\Pi_E^1 v_h, \Pi_E^1 w_h)_{0,E} + h_E^2 S^E(v_h - \Pi_E^1 v_h, w_h - \Pi_E^1 w_h),$$

where S^E is defined in (7). Next we obtain a computable global approximate L^2 form of $(v_h, w_h)_{0,\omega}$,

$$(v_h, w_h)_{h,\omega} = \sum_{E \in \mathcal{T}_h} (v_h, w_h)_{h,E}.$$

Accordingly, the right-hand side of the variational problem (3) is discretised by

$$(f, v_h)_{h,\omega} = \sum_{E \in \mathcal{T}_h} (f, v_h)_{h,E} = \sum_{E \in \mathcal{T}_h} (\Pi_E^0 f, v_h)_{h,E},$$

where $\Pi_E^0 : V_h^E(E) \to \mathbb{P}_0(E)$ denotes the L^2-orthogonal projection onto constants defined by

$$\int_E (v_h - \Pi_E^0 v_h) p dx = 0,\ \forall v_h \in V_h^E(E),\ p \in \mathbb{P}_0(E),$$

which in turn implies that

$$(\Pi_E^0 f, v_h)_{h,E} = \frac{1}{n_E} \int_E \Pi_E^0 f = \frac{|E|}{n_E} f(\mathbf{x}_E).$$

Then we can write a computable discrete problem of (3): find $u_h \in V_h$ such that

$$a_h(u_h, v_h) = (f, v_h)_{h,\omega}, \quad \forall v_h \in V_h.$$

3. Difference virtual element method for 3D elliptic equation

In this section, we present the DVEM method for the 3D elliptic equation with the finite difference solution in the z direction. For convenience, we denote $u(x, y, z)$ by $u(z)$ if there is no confusion. The three-dimensional elliptic equation can be written in the following form:

$$\begin{cases} -\partial_{zz} u - \nabla \cdot (\mathbf{A}(x, y) \nabla u) = f, \text{ in } \Omega, \\ u = 0, \text{ on } \partial\Omega. \end{cases} \tag{8}$$

In the z-direction, $(0, L_3)$ is divided into l_3 equal portions for the 3D domain Ω with the uniform mesh size τ, i.e., $z_k = k\tau, k = 0, ..., l_3$. For the sake of simplicity, we consider $\mathcal{T}_{h\tau} = \cup_{k=0}^{l_3} \mathcal{T}_{hk}$ as a quasi-regular cylindrical mesh with a mesh size of τ in the z-direction. Denote by Z_τ the continuous piecewise linear function space expressed by

$$Z_\tau = \{ v_h(z) \,|\, v_h(z) = \sum_{i=0}^{l_3} v_i \varphi_i(z) \},$$

where φ_i denotes the corresponding 1D piecewise linear basis function, i.e., for $k = 1, 2, ..., l_3 - 1$,

$$\varphi_k(z) = \begin{cases} \dfrac{z - z_{k-1}}{\tau}, & z \in [z_{k-1}, z_k], \\ \dfrac{z_{k+1} - z}{\tau}, & z \in [z_k, z_{k+1}], \\ 0, & z \notin [z_{k-1}, z_{k+1}], \end{cases}$$

for $z \notin [z_{k-1}, z_{k+1}]$, there are $\phi_k(z) = 0, k = 1, \cdots, l_3 - 1$. Define

$$\phi_0(z) = \begin{cases} \dfrac{z_1 - z}{\tau}, & z \in [z_0, z_1], \\ 0, & z \notin [z_0, z_1], \end{cases}$$

and

$$\phi_{l_3}(z) = \begin{cases} \dfrac{z - z_{l_3-1}}{\tau}, & z \in [z_{l_3-1}, z_{l_3}], \\ 0, & z \notin [z_{l_3-1}, z_{l_3}]. \end{cases}$$

Thus we can succinctly define the 3D finite dimensional subspace $X_{h\tau} = V_h \times Z_\tau \subset H_0^1(\Omega)$. Hereafter, c and c_i will denote some needed generic positive constant independent of h and τ with different meaning in different situations.

3.1. Finite difference discretization in the z-direction. Introducing the subspace H_τ^1 of $L^2(\omega)$ in the z-direction,

$$H_\tau^1 := \{v_\tau = \sum_{k=0}^{l_3} v^k(x, y)\varphi_k(z); v^k \in L^2(\omega), k = 0, ..., l_3\},$$

We define the continuous L^2 inner product

$$(u_\tau, v_\tau)_{0,\Omega} = \int_0^{L_3} (u(z), v(z))_{0,\omega} dz,$$

with the induced norm $\|\cdot\|_{0,\Omega}^2 = (\cdot, \cdot)_{0,\Omega}$ and the corresponding discrete counterpart as

$$(u_\tau, v_\tau)_{0,\omega} = \sum_{k=0}^{l_3} \tau(u^k, v^k)_{0,\omega},$$

with the induced norm $\|\cdot\|_{l^2}^2 = (\cdot, \cdot)_{0,\omega}$.

Define the finite difference solution u_τ

$$u_\tau = \sum_{i=1}^{l_3-1} u^k(x, y)\varphi_k(z),$$

where $u^k = u^k(x, y) \in H^2(\omega)$ is solved by

$$-d_{zz}u^k - \nabla \cdot (\mathbf{A}(x, y)\nabla u^k) = f^k, \ k = 1, ..., l_3 - 1, \tag{9}$$

with $u^k|_{\partial\omega} = 0$, $u^0(x, y) = u^{l_3}(x, y) = 0$, $\forall (x, y) \in \omega$, and

$$-d_{zz}u^k = \frac{1}{\tau}(d_z u^{k+1} - d_z u^k), \ d_z u^k = \frac{1}{\tau}(u^k - u^{k-1}).$$

For the purpose of subsequent theoretical proof, we introduce the commonly used discrete Green formula [33, 38].

Lemma 3.1. *Assume $a^k, b^k \in L^2(\omega)$, $k = 1, ..., l_3$ and $b^0 = b^{l_3} = 0$, then there holds that*

$$-\sum_{k=1}^{l_3-1}(a^{k+1}-a^k, b^k)_{0,\omega} = \sum_{k=1}^{l_3}(a^k, b^k - b^{k-1})_{0,\omega}. \tag{10}$$

Furthermore, if $a^k, b^k \in H^1(\omega)$ for $k = 1, ..., l_3$ and $b^0 = b^{l_3} = 0$, we have

$$-\sum_{k=1}^{l_3-1}(\nabla a^{k+1}-\nabla a^k, \nabla b^k)_{0,\omega} = \sum_{k=1}^{l_3}(\nabla a^k, \nabla b^k - \nabla b^{k-1})_{0,\omega}.$$

Assuming $u \in H^3(\Omega)\cap H_0^1(\Omega)$ and $\partial_{zz} f \in L^2((0, L_3); H^{-1}(\omega))$, where $L^2((0, L_3); H^{-1}(\omega))$ represents a space of functions that are square-integrable over the interval $(0, L_3)$ and have a distributional derivative that belongs to $H^{-1}(\omega)$. Now, in order to analyze the approximate properties of u^k regarding $u(z_k)$, we consider $z = z_k$ in (1), we have

$$-d_{zz}u(z_k) - \nabla\cdot(\mathbf{A}(x,y)\nabla u(z_k)) = f^k + E^k, \tag{11}$$

where

$$\begin{aligned} E^k &= -d_{zz}u(z_k) - \nabla\cdot(\mathbf{A}(x,y)\nabla u(z_k)) + \frac{1}{\tau}\int_{z_{k-1}}^{z_k}\partial_{zz}u(z)dz \\ &+\frac{1}{\tau}\int_{z_{k-1}}^{z_k}\nabla\cdot(\mathbf{A}(x,y)\nabla u(z))dz \\ &= -\frac{1}{\tau}(d_z u(z_{k+1}) - \partial_z u(z_k)) + \frac{1}{\tau}(d_z u(z_k) - \partial_z u(z_{k-1})) \\ &-\frac{1}{\tau}\int_{z_{k-1}}^{z_k}(z - z_{k-1})\partial_z\nabla\cdot(\mathbf{A}(x,y)\nabla u(z))dz. \end{aligned}$$

For convenience, we set

$$G^k = -\frac{1}{\tau}\int_{z_{k-1}}^{z_k}(z - z_k)\partial_{zz}u(z)dz,$$

E^k can be expressed as:

$$E^k = -\frac{1}{\tau}(G^{k+1} - G^k) - \frac{1}{\tau}\int_{z_{k-1}}^{z_k}(z - z_{k-1})\partial_z\nabla\cdot(\mathbf{A}(x,y)\nabla u(z))dz.$$

Setting $e^k = u(z_k) - u^k$ and subtracting (8) from (11), we obtain error equation:

$$-\frac{1}{\tau}\Big(d_z e^{k+1} - d_z e^k\Big) - \nabla\cdot(\mathbf{A}(x,y)\nabla e^k) = E^k. \tag{12}$$

It follows from (12) that

$$\begin{aligned} &\sum_{k=1}^{l_3}\tau\|d_z e^k\|_{0,\omega}^2 + \sum_{k=1}^{l_3-1}\tau(\mathbf{A}(x,y)\nabla e^k, \nabla e^k)_{0,\omega} \\ &= \sum_{k=1}^{l_3-1}\tau(E^k, e^k)_{0,\omega} \\ &= \sum_{k=1}^{l_3}\tau(G^k, d_z e^k)_{0,\omega} + \sum_{k=1}^{l_3-1}(\int_{z_{k-1}}^{z_k}(z - z_{k-1})\mathbf{A}(x,y)\nabla\partial_z u(z), \nabla e^k)_{0,\omega}dz. \end{aligned}$$

Based on the assumption of matrix $\mathbf{A}$ and Young's inequality, we have

$$\begin{aligned}
&\sum_{k=1}^{l_3}\tau\|d_z e^k\|_{0,\omega}^2+\alpha_*\sum_{k=1}^{l_3-1}\tau\|\nabla e^k\|_{0,\omega}^2\\
&\le\sum_{k=1}^{l_3}\tau\|G^k\|_{0,\omega}^2+\alpha^*\sum_{k=1}^{l_3-1}(\int_{z_{k-1}}^{z_k}(z-z_{k-1})\|\nabla\partial_z u(z)\|_{0,\omega}^2dz\\
&\le C\tau^2(\|\partial_{zz}u\|_{0,\Omega}^2+\|\nabla\partial_z u\|_{0,\Omega}^2).
\end{aligned}$$

Introducing the following interpolation operator $I_\tau : H_0^1((0,L_3);L^2(\omega))\to X_{h\tau}$ such that

$$I_\tau v(x,y,z)=\sum_{k=1}^{l_3-1}v(x,y,z_k)\phi_k(z)\ \forall v\in H_0^1((0,L_3);L^2(\omega)),$$

we have the following lemma.

Lemma 3.2. [35] *If $v(x,y,z)\in H^2(\Omega)$, then there holds:*

$$\|v-I_\tau v\|_{0,\Omega}^2\le c\tau^4\|v\|_{2,\Omega}^2, \tag{13}$$

$$\|\partial_z(v-I_\tau v)\|_{0,\Omega}^2\le c\tau^2\|v\|_{2,\Omega}^2. \tag{14}$$

Moreover, we have

$$\|\nabla(v-I_\tau v)\|_{0,\Omega}^2\le c\tau^2\|v\|_{2,\Omega}^2. \tag{15}$$

3.2. Difference virtual element method discretization 3D elliptic equation. Now, we define the DVE solution for 3D elliptic equation as follows:

$$u_h(x,y,z)=\sum_{i=1}^{l_3-1}u_h^k(x,y)\varphi_k(z),$$

where $u_h^k(x,y)\in V_h$ is the virtual element approximation of $u^k(x,y)$. Expanding the virtual element solution $u_h^k(x,y)$ as

$$u_h^k(x,y)=\sum_{i=1}^{l_3-1}u_i\phi_i,$$

we get a computable form of (9):

$$-(d_{zz}u_h^k,v_h)_{h,\omega}+a_h(u_h^k,v_h)=(f^k,v_h)_{h,\omega},\ \forall v_h\in V_h, \tag{16}$$

for $k=1,..,l_3-1$.

4. Convergence analysis

In this section, we perform the convergence analysis of the DVEM for the 3D elliptic equation. Firstly, we introduce the H^1 projection operators R_h: $H_0^1(\omega)\to V_h$,

$$(\mathbf{A}(x,y)\nabla R_h u,\nabla v_h)_{0,\omega}=(\mathbf{A}(x,y)\nabla u,\nabla v_h)_{0,\omega}\quad\forall v_h\in V_h.$$

Then for any $u\in H_0^1(\Omega)$ where $\Omega=\omega\times[0,L_3]$, we define 3D finite dimensional interpolation as

$$I_{h\tau}u=R_h(I_\tau u).$$

Lemma 4.1. *The projection operators R_h satisfies the following properties:*

$$\|\nabla R_h u\|_{0,\omega}\le\|\nabla u\|_{0,\omega}\quad\forall u\in H_0^1(\omega),$$
$$\|u-R_h u\|_{0,\omega}+h\|\nabla(u-R_h u)\|_{0,\omega}\le ch^2\|u\|_{2,\omega}\quad\forall u\in H^2(\omega)\cap H_0^1(\omega).$$

We present some useful preliminary results in the sequel, starting with the following approximate lemma.

Lemma 4.2. *Assume $\phi \in H^2(E)$ for any $E \in \mathcal{T}_h$, then it holds*

$$||\phi - \Pi_E^0\phi||_{0,E} + h||\nabla(\phi - \Pi_E^0\phi)||_{0,E} \le ch_E^2|\phi|_{2,E},$$
$$||\phi - \Pi_E^1\phi||_{0,E} + h||\nabla(\phi - \Pi_E^1\phi)||_{0,E} \le ch_E^2|\phi|_{2,E},$$
$$||\phi - \Pi_E^\nabla\phi||_{0,E} + h||\nabla(\phi - \Pi_E^\nabla\phi)||_{0,E} \le ch_E^2|\phi|_{2,E}.$$

Lemma 4.3. *If $u \in H^2(\Omega)$, the interpolation $I_{h\tau}u$ satisfies the following error estimate:*

$$\|\nabla(I_\tau u - I_{h\tau}u)\|_{0,\Omega}^2 + \|\partial_z(I_\tau u - I_{h\tau}u)\|_{0,\Omega}^2 \le c(h^2+\tau^2)\|u\|_{0,\Omega}^2. \tag{17}$$

Proof. According to the properties of the projection operators R_h and Lemma 3.2 and using integration by parts, we obtain

$$\begin{aligned}
&\int_{z_{k-1}}^{z_k} \|\nabla(I_\tau u - I_{h\tau}u)\|_{0,\omega}^2 dz \\
\le &\int_{z_{k-1}}^{z_k} \|\nabla(I_\tau u - u)\|_{0,\omega}^2 + \|\nabla R_h(I_\tau u - u)\|_{0,\omega}^2 + \|\nabla(u - R_h u)\|_{0,\omega}^2 dz \\
\le &\, c_1\tau^2 \int_{z_{k-1}}^{z_k} \|\partial_z \nabla u\|_{0,\omega}^2 dx_4 + c_2 h^2 \int_{z_{k-1}}^{z_k} \|\Delta u\|_{0,\omega}^2 dz,
\end{aligned}$$

and

$$\begin{aligned}
\int_{z_{k-1}}^{z_k} \|\partial_z(I_\tau u - I_{h\tau}u)\|_{0,\omega}^2 dz &\le ch^2 \int_{z_{k-1}}^{z_k} \|\nabla \partial_z I_\tau u\|_{0,\omega}^2 dz \\
&\le ch^2 \int_{z_{k-1}}^{z_k} \|\partial_z \nabla u\|_{0,\omega}^2 dz.
\end{aligned}$$

Summing the above inequality from $k = 1$ to $k = l_3$ yields (17). □

Recalling the definitions of the interpolation operation I_τ and the projection operator R_h. Let $u(z_k) - u_h^k = (I - R_h)u(z_k) + R_h u(z_k) - u_h^k = \eta_h^k + e_h^k$, According to the definition of projection operator Π_E^∇, Π_E^1 and Π_E^0, we can deduce from (11) and (16) that

$$\begin{aligned}
&-(d_{zz}e_h^k, v_h)_{0,\omega} + a(e_h^k, v_h) \\
=&(d_{zz}\eta_h^k, v_h)_{0,\omega} + (E^k, v_h)_{0,\omega} + (I_1^k, v_h)_{0,\omega} + (I_2^k, v_h)_{0,\omega},
\end{aligned} \tag{18}$$

where

$$\begin{aligned}
(I_1^k, v_h)_{0,\omega} &= \sum_{E\in\mathcal{T}_h} ((I - \Pi_E^0)f(z_k), v_h)_{0,E} \le ch^2\|f(z_k)\|_{2,\omega}\|v_h\|_{1,\omega}, \\
(I_2^k, v_h)_{0,\omega} &= \sum_{E\in\mathcal{T}_h} S^E(u_h^k - \Pi_E^\nabla u_h^k, v_h - \Pi_E^\nabla v_h) + h_E^2 S^E(u_h^k - \Pi_E^1 u_h^k, v_h - \Pi_E^1 v_h) \\
&\le ch^2\|u_h^k\|_{1,\omega}\|v_h\|_{1,\omega}.
\end{aligned}$$

Next, we setting $v_h = \tau e_h^k$ to (18), we arrive at

$$\begin{aligned}
-(d_z e_h^{k+1} - d_z e_h^k, e_h^k)_{0,\omega} + \tau a(e_h^k, e_h^k) = &\ (d_z\eta_h^{k+1} - d_z\eta_h^k, e_h^k)_{0,\omega} + \tau(E^k, e_h^k)_{0,\omega} \\
&+\tau(I_1^k, e_h^k)_{0,\omega} + \tau(I_2^k, e_h^k)_{0,\omega}.
\end{aligned} \tag{19}$$

Summing (19) from $k=1$ to l_3-1 and combining (10) in Lemma 3.1, we obtain

(20)
$$\sum_{i=1}^{l_3}\tau\|d_z e_h^k\|_{0,\omega}^2+\sum_{i=1}^{l_3-1}\tau a(e_h^k,e_h^k)=\sum_{i=1}^{l_3-1}\tau(E^k,e_h^k)_{0,\omega}+\sum_{i=1}^{l_3}\tau(d_z\eta_h^k,d_z e_h^k)_{0,\omega}+\sum_{i=1}^{l_3-1}\tau(I_1^k,e_h^k)_{0,\omega}+\tau(I_2^k,e_h^k)_{0,\omega}.$$

Then, we need estimate the right hand of (20). According to Young's inequality and Lemma 4.1 and the discrete Green formula yields

(21)
$$\begin{aligned}&\left|\sum_{i=1}^{l_3-1}\tau(E^k,e_h^k)_{0,\omega}\right|\\&=\left|\sum_{k=1}^{l_3-1}(\int_{z_{k-1}}^{z_k}(z-z_{k-1})\partial_z\mathbf{A}(x,y)\nabla u(z)dz,\nabla e_h^k)_{0,\omega}+\sum_{k=1}^{l_3}\tau(G^k,d_z e_h^k)_{0,\omega}\right|\\&\le\sum_{k=1}^{l_3}\tau^2\int_{z_{k-1}}^{z_k}\|\partial_z\mathbf{A}(x,y)\nabla u(z)\|_{2,\omega}^2dz+\frac{1}{4}\sum_{k=1}^{l_3}\tau\|\nabla e_h^k\|_{0,\omega}^2\\&+\sum_{k=1}^{l_3}\tau\|G^k\|_{0,\omega}^2+\frac{1}{4}\sum_{k=1}^{l_3}\tau\|d_z e_h^k\|_{0,\omega}^2\\&\le c\tau^2\|u\|_{2,\Omega}^2+\frac{1}{4}\sum_{k=1}^{l_3}\tau\|\nabla e_h^k\|_{0,\omega}^2+\frac{1}{4}\sum_{k=1}^{l_3}\tau\|d_z e_h^k\|_{0,\omega}^2,\end{aligned}$$

and

(22)
$$\begin{aligned}\left|\sum_{k=1}^{l_3}\tau(d_z\eta_h^k,d_z e_h^k)_{0,\omega}\right|&\le\sum_{k=1}^{l_3}\tau\|d_z\eta_h^k\|_{0,\omega}^2+\frac{1}{4}\sum_{k=1}^{l_3}\tau\|d_z e_h^k\|_{0,\omega}^2\\&\le h^2\sum_{k=1}^{l_3}\tau\|\nabla d_z u(z_k)\|_{0,\omega}^2+\frac{1}{4}\sum_{k=1}^{l_3}\tau\|d_z e_h^k\|_{0,\omega}^2\\&\le ch^2\|u\|_{2,\Omega}^2+\frac{1}{4}\sum_{k=1}^{l_3}\tau\|d_z e_h^k\|_{0,\omega}^2.\end{aligned}$$

Combining the above inequalities, we have

(23)
$$\sum_{i=1}^{l_3}\tau\|d_z e_h^k\|_{0,\omega}^2+\sum_{i=1}^{l_3-1}\tau a(e_h^k,e_h^k)\le c(h^2+\tau^2).$$

In summary, considering the properties of $a(\cdot,\cdot)$, we conclude the following error estimate result.

Theorem 4.1. *If $u\in H^2(\Omega)$, then the differential virtual element solution u_h satisfies the following error estimates*

$$\|\nabla(u-u_h)\|_{l^2}^2+\|d_z(u-u_h)\|_{l^2}^2\le c(h^2+\tau^2).$$

5. Numerical results

In this section, we perform some numerical examples to demonstrate the efficiency of the DVEM for the 3D elliptic equation on a cylinder domain. Denote the error function $E_h^\tau=u-u_h$. To verify the convergence rate, we calculate the errors of $\|E_h^\tau\|_{0,\Omega}$, $\|\nabla E_h^\tau\|_{0,\Omega}$ and $\|\partial_z E_h^\tau\|_{0,\Omega}$ respectively.

5.1. Convex polyhedron domain. Example 1. In this test, we take the coefficient matrix $\mathbf{A}(x,y)$ as a piecewise constant, and the exact solution is continuous but not smooth everywhere in the (x,y)-plane. We consider unit cubic domain $\Omega = \omega \times [0, L_3] = [0,1]^3$. The exact solution u is as follows:

$$u(x,y,z) = \begin{cases} \frac{4}{9}xyz(z-1), & x < \frac{1}{2}, y < \frac{1}{2}, \\ \frac{2}{3}x(\frac{4}{3}y - \frac{1}{3})z(z-1), & x < \frac{1}{2}, y > \frac{1}{2}, \\ \frac{2}{3}y(\frac{4}{3}x - \frac{1}{3})z(z-1), & x > \frac{1}{2}, y < \frac{1}{2}, \\ (\frac{4}{3}x - \frac{1}{3})(\frac{4}{3}y - \frac{1}{3})z(z-1), & x > \frac{1}{2}, y > \frac{1}{2}, \end{cases}$$

$$\mathbf{A}(x,y) = \begin{cases} 4, \ x < \frac{1}{2}, y < \frac{1}{2}, \\ 2, \ x < \frac{1}{2}, y > \frac{1}{2}, \\ 2, \ x > \frac{1}{2}, y < \frac{1}{2}, \\ 1, \ x > \frac{1}{2}, y > \frac{1}{2}. \end{cases}$$

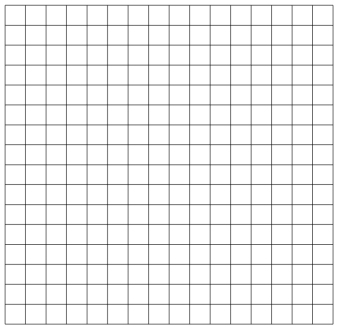

Figure 1: Uniform quadrilateral meshes.

Table 1: Errors and the corresponding convergence rates of DFEM with uniform quadrilateral meshes.

Mesh	$\|E_h^\tau\|_{0,\Omega}$	Order	$\|\nabla E_h^\tau\|_{0,\Omega}$	Order	$\|\partial_z E_h^\tau\|_{0,\Omega}$	Order
$(h,\tau)/2$	8.645e-3	-	5.905e-2	-	5.348e-2	-
$(h,\tau)/4$	2.173e-3	1.992	2.989e-2	0.982	2.675e-2	0.995
$(h,\tau)/8$	5.432e-4	2.000	1.495e-2	1.000	1.337e-2	1.001
$(h,\tau)/16$	1.358e-4	2.000	7.469e-3	1.001	6.683e-3	1.000
$(h,\tau)/32$	3.395e-5	2.000	3.734e-3	1.000	3.341e-3	1.000

Table 2: Errors and the corresponding convergence rates of DVEM with uniform quadrilateral meshes.

Mesh 1	$\|E_h^\tau\|_{0,\Omega}$	Order	$\|\nabla E_h^\tau\|_{0,\Omega}$	Order	$\|\partial_z E_h^\tau\|_{0,\Omega}$	Order
$(h,\tau)/2$	1.046e-2	-	3.523e-2	-	3.229e-2	-
$(h,\tau)/4$	2.647e-3	1.984	1.769e-2	0.994	1.617e-2	0.998
$(h,\tau)/8$	6.619e-4	1.999	8.846e-3	0.999	8.052e-3	1.006
$(h,\tau)/16$	1.580e-4	2.066	4.409e-3	1.005	4.026e-3	1.000
$(h,\tau)/32$	3.924e-5	2.010	2.205e-3	1.000	2.012e-3	1.000

Given the uniform quadrilateral meshes (Figure 1), we begin to test the error results of the DVEM in comparison with the DFEM (see [39]). Table 1 and Table 2 demonstrate the error results computed by DVEM and DFEM, respectively. It can be observed that both methods achieve the optimal convergence rate (1 for $\|\nabla E_h^\tau\|_{0,\Omega}$ and $\|\partial_z E_h^\tau\|_{0,\Omega}$ and 2 for $\|E_h^\tau\|_{0,\Omega}$), which is also in good agreement with the theoretical result in consistent with Theorem 4.1. We also test the DVEM for

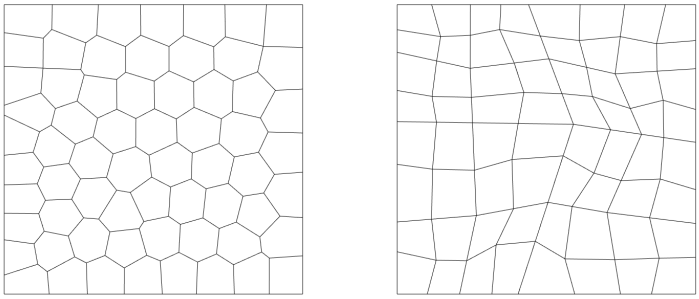

Figure 2: Polyhedron meshes. Left: smooth Voronoi meshes. Right: arbitrary quadrilateral meshes.

Table 3: Errors and the corresponding convergence rates of DVEM with smoothed Voronoi meshes.

Mesh	$\|E_h^\tau\|_{0,\Omega}$	Order	$\|\nabla E_h^\tau\|_{0,\Omega}$	Order	$\|\partial_z E_h^\tau\|_{0,\Omega}$	Order
$(h,\tau)/8$	1.392e-2	-	4.315e-2	-	3.894e-2	-
$(h,\tau)/15$	4.079e-3	1.953	2.324e-2	0.984	2.091e-2	0.989
$(h,\tau)/30$	1.021e-3	1.998	1.163e-2	1.000	1.045e-2	1.001

the 3D elliptic equation with smooth Voronoi meshes and arbitrary quadrilateral meshes (see Figure 2). The corresponding error results and convergence rates of $\|E_h^\tau\|_{0,\Omega}$, $\|\nabla E_h^\tau\|_{0,\Omega}$ and $\|\partial_z E_h^\tau\|_{0,\Omega}$ are displayed in Tables 3-4. From these tables we can see the same convergence result as in the uniform quadrilateral meshes, which shows the advantage of VEM on the polygonal meshes.

Example 2. In this test, we consider the DVEM for 3D elliptic equation in non-convex meshes. With the same referential settings in Example 1, the exact

Table 4: Errors and the corresponding convergence rates of DVEM with arbitrary quadrilateral meshes.

Mesh	$\|E_h^\tau\|_{0,\Omega}$	Order	$\|\nabla E_h^\tau\|_{0,\Omega}$	Order	$\|\partial_z E_h^\tau\|_{0,\Omega}$	Order
$(h,\tau)/4$	4.659e-2	-	1.6976e-1	-	1.283e-1	-
$(h,\tau)/8$	1.172e-2	1.991	8.497e-2	0.998	6.427e-2	0.997
$(h,\tau)/16$	2.934e-3	1.998	4.253e-2	0.999	3.192e-2	1.001
$(h,\tau)/32$	7.331e-4	2.001	2.043e-2	1.056	1.596e-2	0.999

solution is set to be

$$u(x,y,z) = (1-x)(1-y)(1-z)\sin(\pi xyz)e^{x+2z}.$$

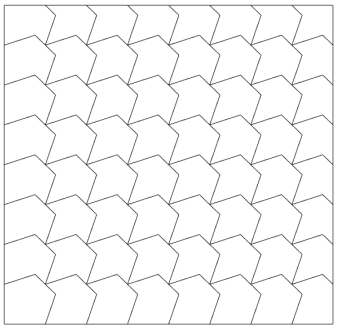

Figure 3: Non-convex meshes.

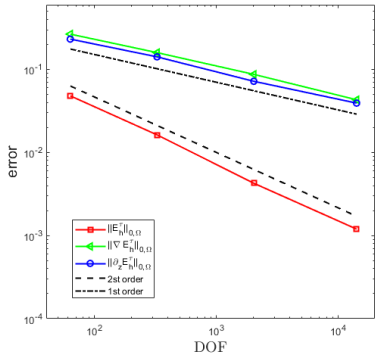

Figure 4: The error results of DVEM for 3D elliptic equation in non-convex meshes with different degrees of freedom in 2D domain ω.

Figure 4 reports the error results and corresponding convergence rate in $\|E_h^\tau\|_{0,\Omega}$, $\|\nabla E_h^\tau\|_{0,\Omega}$ and $\|\partial_z E_h^\tau\|_{0,\Omega}$. We can see the same results as in Example 1, which further illustrates the efficiency of the DVEM in treating the non-convex polyhedral meshes.

5.2. Non-convex polyhedron domain. Example 3. Next, we consider a non-convex L-shaped domain $\Omega = [0,1]^2/[0.5,1]^2 \times [0,5]$. The mesh size in the z-direction is set as $\tau = 5h$. The exact solution is given by:

$$u(x,y,z) = z^2(z-5)^2(x^2 - \tfrac{3}{2}x + \tfrac{1}{2})(y^2 - \tfrac{3}{2}y + \tfrac{1}{2})\sin(\pi xyz).$$

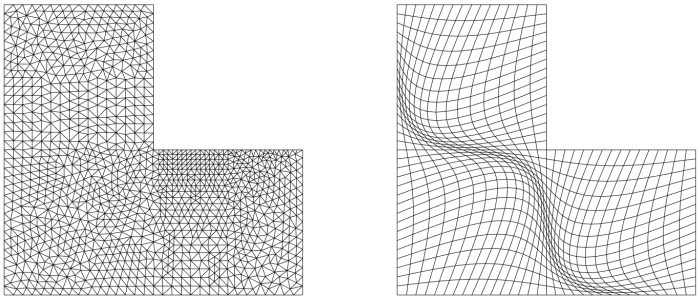

Figure 5: L-shaped domain. Left: non-uniform triangulation meshes. Right: twisted quadrilateral meshes.

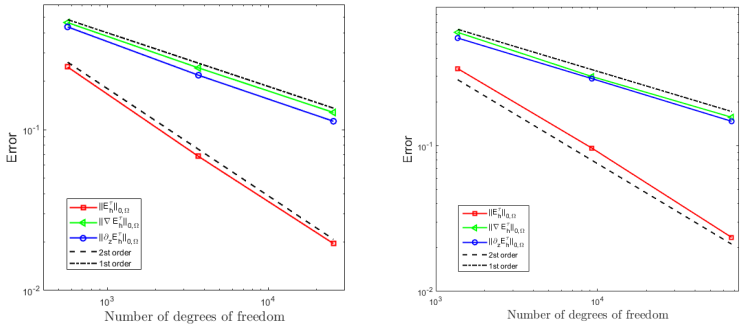

Figure 6: The convergence rates in non-convex L-shaped domain. Left: non-uniform triangulation meshes. Right: twisted quadrilateral meshes.

We consider the non-uniform triangulation meshes and twisted quadrilateral meshes in non-convex L-shaped domain Ω (see Figure 5). The corresponding error results in $\|E_h^\tau\|_{0,\Omega}$, $\|\nabla E_h^\tau\|_{0,\Omega}$ and $\|\partial_z E_h^\tau\|_{0,\Omega}$ are plotted in Figure 6. It can be observed that the optimal convergence orders are achieved, which again shows the efficiency of DVEM in non-convex domains.

Example 4. Finally, we consider the 3D elliptic equation on Wrench domain (see Figure 7). The exact solution is given by:

$$u(x,y,z) = \varphi(x,y)(2\varphi_y(x,y)\xi(z) - \varphi(x,y)\xi'(z)).$$

where $\varphi(x,y) = x^2 + y^2 - 1$, $\xi(z) = z^2(z-1)^2$ and $\varphi_s(x,y)$ denotes the derivative of $\varphi(x,y)$ with respect to s.

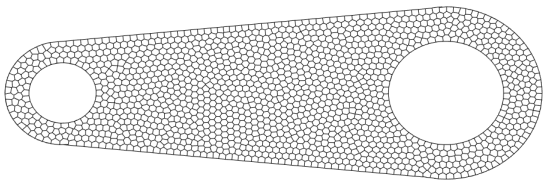

Figure 7: Wrench domain.

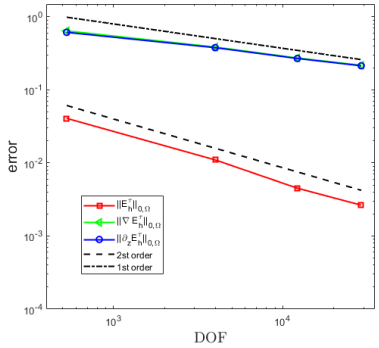

Figure 8: The convergence rates in wrench domain.

Figure 8 shows the error results in $\|E_h^\tau\|_{0,\Omega}$, $\|\nabla E_h^\tau\|_{0,\Omega}$ and $\|\partial_z E_h^\tau\|_{0,\Omega}$ from which we can see the convergence rate is about 1.8 in $\|E_h^\tau\|_{0,\Omega}$ and 0.8 in $\|\nabla E_h^\tau\|_{0,\Omega}$ and $\|\partial_z E_h^\tau\|_{0,\Omega}$, which further proves that DVEM is very effective for complex regions.

6. Conclusions

In this paper, we develop a difference virtual element method for 3D elliptic equation. The proposed method transform a three dimensional problem into a series of two dimensional instances, optimizing computational complexity and enhancing the flexibility of the virtual element method in application to the high-dimensional problems. Also DVEM can be regarded as the generalized form of DFEM, thus has a great flexibility in polygonal meshes, especially for non-convex domains. A variety of numerical examples are carried out to verify the theoretical results. The extension to the incompressible flows and other problems and coupling with adaptive methods will be studied in the future.

Acknowledgments

The authors would like to thank the referees for valuable comments which greatly improved an early version of the paper. This research was supported by the Natural Science Foundation of China (No.12071406).

References

[1] R. Eymard, T. Gallouët and R. Herbin, Finite volume methods. Handbook of numerical analysis, 7: 713-1018, 2000.

[2] F. Darwish, L. Moukalled and M. Mangani, The finite volume method in computational fluid dynamics. 2016.

[3] C. A. Hieber and S. F. A. Shen, finite-element/finite-difference simulation of the injection-molding filling process. Journal of Non-Newtonian Fluid Mechanics, 7(1): 1-32, 1980.
[4] S. C. Brenner. The mathematical theory of finite element methods. Springer, 2008.
[5] A. Quarteroni, A. Valli. Numerical approximation of partial differential equations. Springer Science & Business Media, 2008.
[6] Y. He and J. Li. A stabilized finite element method based on local polynomial pressure projection for the stationary Navier-Stokes equations. Applied Numerical Mathematics, 58(10): 1503-1514, 2008.
[7] Y. He and J. Li. A penalty finite element method based on the Euler implicit/explicit scheme for the time-dependent NavierCStokes equations. Journal of computational and applied mathematics, 235(3): 708-725, 2010.
[8] L. Beirrão da Veiga, F. Brezzi, A. Cangiani, G. Manzini, L. D. Marini, and A. Russo. Basic principles of virtual element methods. Mathematical Models and Methods in Applied Sciences, 23(01):199-214, 2013.
[9] E. Cáceres and G. N. Gatica. A mixed virtual element method for the pseudostress-velocity formulation of the Stokes problem. IMA Journal of Numerical Analysis, 37(1):296-331, 2017.
[10] D. Frerichs and C. Merdon. Divergence-preserving reconstructions on polygons and a really pressure-robust virtual element method for the Stokes problem. IMA Journal of Numerical Analysis, 42(1):597-619, 2022.
[11] E. Cáceres, G. N. Gatica and F. A. Sequeira. A mixed virtual element method for the Brinkman problem. Mathematical Models and Methods in Applied Sciences, 27(04):707C743, 2017.
[12] D. Mora, C. Reales and A. Silgado. A C^1-virtual element method of high order for the Brinkman equations in stream function formulation with pressure recovery. IMA Journal of Numerical Analysis, 42(4):3632-3674, 2022.
[13] G. Vacca. An H^1-conforming virtual element for Darcy and Brinkman equations. Mathematical Models and Methods in Applied Sciences, 28(01):159-194, 2018.
[14] G. Wang, F. Wang, L. Chen and Y. He. A divergence free weak virtual element method for the Stokes-Darcy problem on general meshes. Computer Methods in Applied Mechanics and Engineering, 344:998-020, 2019.
[15] L. Beirão da Veiga, F. Dassi, and G. Vacca. The Stokes complex for virtual elements in three dimensions. Mathematical Models and Methods in Applied Sciences, 30(03):477-512, 2020.
[16] L. Beirão da Veiga, D. Mora and G. Vacca. The Stokes complex for virtual elements with application to Navier-Stokes flows. Journal of Scientific Computing, 81:990-1018, 2019.
[17] L. Beirãoo da Veiga, F. Dassi, G. Manzini and L. Mascotto. The virtual element method for the 3D resistive magnetohydrodynamic model. Mathematical Models and Methods in Applied Sciences, 33(03):643-686, 2023.
[18] D. Mora and A. Silgado. A C^1 virtual element method for the stationary quasi-geostrophic equations of the ocean. Computers & Mathematics with Applications, 116:212-228, 2022.
[19] S. Cao, L. Chen, R. Guo and F. Lin. Immersed virtual element methods for elliptic interface problems in two dimensions. Journal of Scientific Computing, 93(1):12, 2022.
[20] L. Chen, H. Wei and M. Wen. An interface-fitted mesh generator and virtual element methods for elliptic interface problems. Journal of Computational Physics, 334:327-348, 2017.
[21] S. Gómez, L. Mascotto, A. Moiola and I. Perugia. Space-time virtual elements for the heat equation. SIAM Journal on Numerical Analysis, 62(1):199-228, 2024.
[22] J. Tushar, A. Kumar and S. Kumar. Virtual element methods for general linear elliptic interface problems on polygonal meshes with small edges. Computers & Mathematics with Applications, 122:61-75, 2022.
[23] H. Wang, F. Wang, J. Chen and H. Ji. A conforming virtual element method based on unfitted meshes for the elliptic interface problem. Journal of Scientific Computing, 96(1):21, 2023.
[24] T. Arobogast, C. N. Dawson, P. T. Keenan, M. F. Wheeler and I. Yotov. Enhanced cell-centered finite differences for elliptic equations on general geometry. SIAM Journal on Scientific Computing, 19(2):404-425, 1998. 19
[25] Y. He and X. Feng. H^1 stability and convergence of the FE, FV and FD methods for an elliptic equation. East Asian Journal on Applied Mathematics, 3(2):154-170, 2013.
[26] Y. Kuznetsov, K. Lipnikov and M. Shashkov. The mimetic finite difference method on polygonal meshes for diffusion-type problems. Computational Geosciences, 8(4):301-324, 2004.
[27] B. S. Jovanović. Finite difference schemes for partial differential equations with weak solutions and irregular coefficients. Computational Methods in Applied Mathematics, 4(1):48-65, 2004.

[28] K. Li and X. Shen. A dimensional splitting method for the linearly elastic shell. International Journal of Computer Mathematics, 84(6):807-824, 2007.
[29] Y. Hou and H. Wei. Dimension splitting algorithm for a three dimensional elliptic equation. International Journal of Computer Mathematics, 89(1):112-127, 2012.
[30] K. Li, A. Huang and W. Zhang. A dimension split method for the 3D compressible Navier-Stokes equations in turbomachine. Communications in Numerical Methods in Engineering, 18(1):1-14, 2002.
[31] E. Hansen and A. Ostermann. Dimension splitting for evolution equations. Numerische Mathematik, 108(4):557-570, 2008.
[32] H. Chen, K. Li and S. Wang. A dimension split method for the incompressible Navier-Stokes equations in three dimensions. International Journal for Numerical Methods in Fluids, 73(5):409- 435, 2013.
[33] X. Feng, R. He and Z. Chen. H^1-superconvergence of finite difference method based on Q_1-element on quasi-uniform mesh for the 3D Poisson equation. Numerical Methods for Partial Differential Equations, 36(1):29-48, 2020.
[34] X. Feng, R. He and Z. Chen. Superconvergence in H^1-norm of a difference finite element method for the heat equation in a 3D spatial domain with almost-uniform mesh. Numerical Algorithms, 86(1):357-395, 2021.
[35] X. Lu, P. Huang, X. Feng and Y. He. A stabilized difference finite element method for the 3D steady Stokes equations. Applied Mathematics and Computation, 430:127270, 2022.
[36] X. Feng, X. Lu, and Y. He. Difference finite element method for the 3D steady Navier-Stokes equations. SIAM Journal on Numerical Analysis, 61(1):167-193, 2023.
[37] X. Lu, P. Huang, X. Feng and Y. He. A stabilized difference finite element method for the 3D stead incompressible Navier-Stokes equations. Journal of Scientific Computing, 92(3):104, 2022.
[38] R. He, Xinlong Feng, and Zhangxin Chen. H^1-superconvergence of a difference finite element method based on the P_1-P_1-conforming element on non-uniform meshes for the 3D Poisson equation. Mathematics of Computation, 87(312):1659-1688, 2018.
[39] J. Song, D. Sheen, X. Feng and Y. He. A difference finite element method based on nonconforming finite element methods for 3D elliptic problems. (unpubl. MS), 2023.

College of Mathematics and Systems Science, Xinjiang University, Urumqi 830046, PR China
E-mail: lulisay123@sina.com

School of Mathematics and Statistics, Xi'an Jiaotong University, Xi'an 710049, China
E-mail: heyn@mail.xjtu.edu.cn

College of Mathematics and Systems Science, Xinjiang University, Urumqi 830046, PR China
E-mail: fxlmath@xju.edu.cn